CRYSTAL GROWTH & DESIGN

Article

pubs.acs.org/crystal

Sodium Salts and Solvate of Rebamipide: Synthesis, Structure, and Pharmacokinetic Study

Yingnan Chi,[†,∥] Chuanrong Liu,[†,∥] Tianming Ren,[‡] Xiaoying Wang,[†] Qiuhong Yang,[†] Zhichao Yang,[‡] Yan Yang,[‡] Song Yang,[†] Jingkai Gu,[*,‡] and Changwen Hu[*,†]

[†]Key Laboratory of Cluster Science, Ministry of Education of China, Beijing Key Laboratory of Photoelectronic/Electrophotonic, School of Chemistry, Beijing Institute of Technology, Beijing 100081, P. R. China

[‡]Research Center for Drug Metabolism, Jilin University, Changchun 130012, P. R. China

Supporting Information

ABSTRACT: Two sodium salts ($Na(CH_3CH_2OH)$ (HReb) (**1**) and $Na_2(H_2O)_4$(Reb) (**2**)), one methanol solvate (H_2Reb·CH_3OH (**3**)), and one methyl ester (**4**) of the minimally soluble drug, rebamipide (H_2Reb), used for the treatment of gastric ulcers and gastritis have been synthesized. For the first time the structure of rebamipide has been determined by single crystal X-ray diffraction. Although salts **1** and **2** were prepared under the similar conditions, their structures are different. In **1**, rebamipide loses the proton of the carboxyl group to interact with the sodium ion, but in **2** the drug molecule converts to its prototropic tautomer and then simultaneously loses the protons of the carboxyl and hydroxyl groups to form salt. Control experiments show that reaction temperature is the key factor influencing the formation of salts. Although all methanol was used in the synthesis of **3** and **4**, in **3** methanol acts as solvent involved in the lattice, while in **4** it reacts with rebamipide to form ester. By analyzing the mass spectra of the reaction solution, we speculate that the crystallization of **3** and **4** is controlled by the product's solubility. Dissolution studies indicate that both the maximum solubility and dissolution rate of **1**−**4** in simulated succus gastricus are improved. Furthermore, pharmacokinetic behavior of compounds **1**−**4** was investigated in rats and the results indicate that the bioavailability of **1**, **3**, and **4** upon oral administration is enhanced compared to that of API.

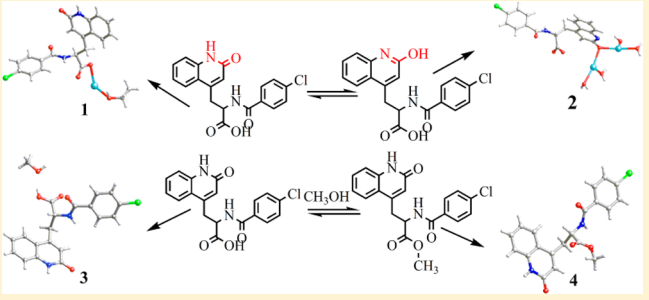

INTRODUCTION

Rebamipide, an amino acid derivative of 2-(1*H*)-quinolinone, is a therapeutic agent for gastric ulcers and chronic gastritis. It was first synthesized by Otsuka Pharmaceutical Company, Ltd. in 1985[1] and subsequently marketed with the trade name of Mucosta in 1990. The molecular structure of rebamipide is shown in Scheme 1. This drug can stimulate the generation of endogenous prostaglandins in the gastric mucosa, thereby facilitating and accelerating ulcer healing.[2] In addition, recent clinical studies display that rebamipide can effectively treat stomatitis, colitis, and dry eye syndrome.[3−5] According to the Biopharmaceutics Classification System (BCS), rebamipide belongs to the Class IV drugs, which have low solubility and low permeability.[6] Rebamipide is nearly insoluble in most common organic solvents and its solubility in water is approximately 0.0001 and 0.013% (w/v) at pH 3 and 7, respectively.[7] As a result, the absorption of this drug is poor with the absolute bioavailability of about 10%.[8]

Scheme 1. Molecular Structure of Rebamipide

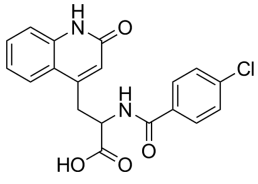

Recently, solid state forms, referring to polymorphs, solvates (or hydrates), salts, cocrystals, or amorphous forms, play an important role in the pharmaceutical field.[9−12] A lot of studies demonstrate that many physical and chemical properties of an active pharmaceutical ingredient (API), such as stability,[13,14] solubility,[15−22] and bioavailability,[23−25] are influenced by the selection and optimization of solid state forms. The reported solid state forms of rebamipide include one monohydrate,[26] two cocrystals,[27] and several salts.[28] Forming salt is the classic method for improving solubility and dissolution rate of acidic/basic APIs.[25,29−31] Although choline, arginine, lysine, trometh-amine, sodium, calcium, zinc, and magnesium salts of rebamipide were synthesized in patent, no structural characterization was provided.[28] With the existence of two acidic functional groups in rebamipide, a carboxylic acid and a *N*-heterocycle, it is not easy to predict the product when reacting with alkaline agents. A careful

Received: December 30, 2015
Revised: April 14, 2016

DOI: 10.1021/acs.cgd.5b01839
Cryst. Growth Des. XXXX, XXX, XXX−XXX

Table 1. Crystallographic Data for Compounds 1−4[a]

	1	2	3	4
formula	$C_{21}H_{20}ClN_2NaO_5$	$C_{19}H_{21}ClN_2Na_2O_8$	$C_{20}H_{19}ClN_2O_5$	$C_{20}H_{17}ClN_2O_4$
formula weight	438.83	486.81	402.82	384.81
crystal system	monoclinic	orthorhombic	monoclinic	monoclinic
space group	*P*21/*c*	*Pna*2(1)	*C*2/*c*	*P*21*c*
a (Å)	6.014(2)	34.551(3)	23.030(2)	19.7573(15)
b (Å)	23.279(9)	5.0944(4)	19.1331(18)	5.0379(3)
c (Å)	15.076(6)	12.0785(11)	9.6060(9)	19.5600(12)
α (deg)	90	90	90	90
β (deg)	99.969(7)	90	106.358(2)	109.887(7)
γ (deg)	90	90	90	90
Z	4	4	8	4
volume (Å^3)	2078.9(14)	2126.0(3)	4061.4(7)	1830.8(2)
D_{calc} (g·cm^{-3})	1.402	1.521	1.318	1.396
F (000)	912	1008	1680	800
refns. collected	10139	9761	10191	8493
unique reflns.	3637	2869	3572	3382
R_{int}	0.0447	0.0708	0.0599	0.0258
$R_1[I > 2\sigma(I)]$	0.0634	0.0470	0.0612	0.0651
$wR_2[I > 2\sigma(I)]$	0.2021	0.1020	0.1437	0.1702
R_1(all data)	0.1092	0.0581	0.1261	0.0898
wR_2 (all data)	0.2620	0.1056	0.1618	0.1877
GOF on F^2	1.052	1.060	1.044	1.065

[a] $R_1 = \sum| |F_o| - |F_c| |/\sum|F_o|$; $wR_2 = \sum[w(F_o^2 - F_c^2)^2]/\sum[w(F_o^2)^2]^{1/2}$

literature and Cambridge Structural Database (CSD) search indicates that although rebamipide has been widely investigated since 1985, so far no crystal structure of rebamipide or its salt, hydrate, solvate, or cocrystal is reported. However, unambiguous structural characterization is necessary in the development of a drug, which is helpful to build the structure−property relationship and guide the controllable synthesis.

Herein, for the first time we determine the crystal structures of two rebamipide sodium salts, namely Na(CH_3CH_2OH) (HReb) (**1**) and $Na_2(H_2O)_4$(Reb) (**2**), and one methanol solvate, H_2Reb·CH_3OH (**3**) (H_2Reb = rebamipide). Moreover, during the screening of solid state form, the single crystal of rebamipide methyl ester (**4**) has been fortunately obtained. In addition, compounds **1**−**4** have been characterized by powder X-ray diffraction, Fourier transform-infrared spectroscopy (FT-IR), thermogravimetry, and differential scanning calorimetry. It is notable that both the maximum solubility and bioavailability of **1**, **3**, and **4** are enhanced compared to those of API.

EXPERIMENTAL SECTION

Materials and General Methods. Rebamipide (purity >98%) was provided by Research Center for Drug Metabolism of Jilin University and used without further purification. The other chemicals were reagent grade, purchased from commercial sources, and used without further purification. IR spectra were obtained (as KBr-pressed pellets) using a Nicolet 170SXFT/IR spectrometer in the range of 500−4000 cm^{-1}. Powder X-ray diffraction (PXRD) data were collected on a Bruker instrument equipped with graphite-monochromatized Cu K*α* radiation (*λ* = 0.154060 nm, scan speed = 8°/min, 2*θ* = 5−35°, stepsize = 0.019762). TG analyses were carried out in nitrogen atmosphere between 30 and 350 °C at a heating rate of 10 °C/min on a SDT Q600 simultaneous thermal analyzer. Differential scanning calorimetry was performed on a Q100 DSC module with nitrogen flow rate of 50 mL·min^{-1}. ^{1}H NMR spectra were recorded using a Bruker-400 NMR spectrometer. Mass spectra were recorded in the positive mode on an Agilent 6520 Q-TOF LC/MS mass spectrometer. Sample solutions were made to approximately 10^{-6} M in ultrapurified water or methanol and transferred to the electrospray source via an autosampler with a flow rate of 0.2 mL/min.

Synthesis of Na(CH_3CH_2OH) (HReb) (1). Rebamipide (100 mg, 0.27 mmol) was dissolved in 15 mL ethanol and then stirred for 2 h. To this was added 0.075 mL NaOH (5 M) with vigorously stirring. The resulting solution was filtered and allowed for slow evaporation under ambient conditions. Colorless block single crystals of **1** suitable for single X-ray diffraction were obtained and dried under ambient conditions (yield of 95 mg, ∼80% based on rebamipide).

Synthesis of $Na_2(H_2O)_4$(Reb) (2). Compound **2** was prepared using a procedure similar to that for **1**. The only difference is that the mixture of rebamipide and sodium hydroxide solution was heated at 50 °C for 30 min, then filtered and allowed for crystallization. After 1 day, colorless needle-like single crystals of **2** were isolated and dried at ambient conditions (yield of 98 mg, ∼75% based on rebamipide).

Synthesis of H_2Reb·CH_3OH (3). Rebamipide (45 mg, 0.12 mmol) was dissolved in 15 mL methanol and stirred for 2 h. The solution was then transferred to a Teflon-lined autoclave (15 mL) and kept at 120 °C for 48 h. After the mixture was slowly cooled to room temperature, the resulting solution was filtered and slowly evaporated at ambient conditions. After 2 days, colorless needle-shaped crystals of **3** were harvested (yield of 40 mg, ∼82% based on rebamipide) and one single crystal was chosen for X-ray analysis.

Synthesis of Rebamipide Methyl Ester (4). Compound **4** was synthesized using a procedure similar to that of **3**. The only difference is that the API was dissolved in the methanol-H_2O (v:v = 3:1) solution. The obtained solution was heated at 120 °C in a Teflon-lined autoclave (15 mL) for 48 h, and then the resulting solution was allowed to evaporate at ambient conditions. Colorless block crystals of **4** were isolated after about 7 days (yield 35 mg, ∼75% based on rebamipide). ^{1}H NMR (DMSO-d_6, 400 MHz) *δ* (ppm) 11.66 (1H, s, imino group), 9.03 (1H, d, imino group), 7.21−7.85 (8H, m, phenyl), 6.44 (1H, s, alkenyl), 4.35 (1H, t, methine), 3.69 (3H, s, methyl), 2.06 (2H, s, methylene). (Supporting Information, Figure S1)

Single Crystal X-ray Diffraction. The single crystal data for compounds **1**−**4** were collected on a Bruker-AXS CCD diffractometer equipped with a Mo K*α* radiation source (*λ* = 0.07103 Å) at 298 K. The absorption corrections were performed with the SADABS program. The structures were determined by direct methods and expanded using Fourier techniques. The non-hydrogen atoms were refined

DOI: 10.1021/acs.cgd.5b01839
Cryst. Growth Des. XXXX, XXX, XXX−XXX

Table 2. Hydrogen Bonding Interactions in Compounds 1−4

D−H···A	D−H/Å	H···A/Å	D···A/Å	D−H···A/°	symmetry code
compound **1**					
N1−H1···O1	0.860	2.004	2.858	172.05	−x+2, −y+1, -z+1
N2−H2A···O1	0.860	2.338	3.102	148.23	x−1, y, z
O5−H5A···O4	0.849	1.818	2.685	169.92	x−1, y, z
compound **2**					
N2−H2A···O2	0.860	2.333	3.175	166.11	x, y−1, z
O5−H5A···O1	0.970	1.886	2.720	142.54	−x+1, −y, z−1/2
O5−H5B ···N1	0.970	2.492	3.203	130.03	−x+1, −y+1, z−1/2
O6−H6A···N1	0.850	2.078	2.920	170.47	x, y−1, z
O6−H6B···O4	0.850	2.036	2.839	157.29	−x+1, −y, z−1/2
O7−H7A···O8	0.970	1.964	2.726	133.78	intramolecular
O7−H7B···N1	0.970	2.262	2.871	119.81	−x+1, −y, z−1/2
O8−H8A···O4	0.852	1.922	2.772	174.68	−x+1, −y, z−1/2
O8−H8B···O2	0.851	1.961	2.785	162.71	−x+1, −y+1, z−1/2
compound **3**					
N1−H1···O3	0.860	2.026	2.883	174.03	−x+3/2,y+1/2,−z+1/2
N2−H2A···O2	0.860	2.122	2.869	144.90	x, −y+1, z−1/2
O4−H4B···O5	0.850	1.782	2.609	163.88	intramolecular
O5−H5A···O1	0.820	1.979	2.701	146.53	−x+3/2,y−1/2, −z+1/2
O5−H5B···O1	0.850	2.018	2.701	136.78	−x+3/2,y−1/2, −z+1/2
compound **4**					
N1−H1···O1	0.860	1.972	2.826	172.10	x, y−1, z
N2−H2A···O2	0.860	2.007	2.923	167.62	−x,y+1/2,−z−1/2

anisotropically. The H atoms on C atoms were fixed at the calculated positions and those on the water molecules were located from the different Fourier maps. The H atoms were isotropically refined. All calculations were performed using the SHELXTL-97 program.[32] CCDC-1439505 (**1**) 1404896 (**2**) 1404894 (**3**) and 1439500 (**4**) contain the supplementary crystallographic data for this paper. The crystallographic details of the compounds are summarized in Table 1. The hydrogen bonding distances and angles are present in Table 2 and the selected bond length and angles are given in Table S2.

Dissolution and Solubility. The absorbance of a known concentration of rebamipide was measured at the given λ_{max} (228 nm) using a TU-1901 UV−vis spectrometer. The absorbance values were plotted against several known concentrations to prepare the concentration vs intensity calibration curve (R^2 = 0.9996). From the slopes of the calibration curves, the molar extinction coefficients of compounds **1**−**4** were calculated. The rebamipide derivatives were milled to powders and sieved using standard mesh sieves to provide samples with the approximate particle size distribution of 75−150 μm. In order to determine the equilibrium solubility, an excess amount of compound was added to 10 mL of simulated gastric fluid media (HCl solution with pH = 1.2). The supersaturated solution was stirred (50 rpm) at room temperature. The suspension was filtered through a 0.22 μm nylon filter after 24 h. The filtered aliquots were diluted and the absorbance was measured at the given λ_{max}.

In the dissolution experiment, 50 mL of HCl solution (pH = 1.2) was added to a 100 mL flask containing excess powder samples, and the resulting mixture was stirred at 25 °C and 500 rpm. The solution was withdrawn from the flask at regular intervals and filtered through a 0.22 μm nylon filter. The concentration of the aliquots was determined with appropriate dilutions measured with UV−vis spectrophotometry. Each experiment was conducted three times and the mean value in each case was calculated.

Pharmacokinetic Study (PK). The pharmacokinetics of compounds **1**−**4** and original API were conducted using Wistar rats. After an overnight fast, 15 healthy rats (7 months, weighing 220−260 g) were randomly divided into five groups before dosing. Pure powder samples of rebamipide API and compounds **1**−**4** as oral formulations were administered to rats in different groups by gastric perfusion using a dry powder insufflator at a single dose of 12 mg/kg for each group. Subsequently, 0.5 mL aliquots of whole blood samples were collected from the eyeball veins at intervals of 0.17, 0.33, 0.5, 0.75, 1, 2, 3, 5, 7, 9, 11, and 24 h from each rat, immediately centrifuged for 5 min at 13300 rpm at ambient temperature, and stored at −20 °C until LC−MS/MS analysis. Analysis was performed on a LC−MS/MS system comprising Agilent 1100 Series HPLC system (Agilent Technologies, Palo Alto, CA, USA) and a Q-trap 2000 mass spectrometer (Applied BiosystemsSciex, Ontario, Canada). Chromatographic separation was achieved using an Agilent ZORBAX 300 SB-C18 column (150 mm × 4.6 mm I.D., 5 μm particle size) at 40 °C with a mobile phase of formic acid/water (v/v = 70:30) at 1 mL/min. Analysis was carried out with an electrospray ionization (ESI) source using positive ion mode. Data were acquired using Drug and Statistics Software DAS 3.0 (Mathematical Pharmacology Professional Committee of China, Shanghai, China). The hydrolysis experiment of compound **4** in vivo has been performed using the similar method.

RESULTS AND DISCUSSION

Crystal Structure of Na(CH_3CH_2OH) (HReb) (1). When reacting with NaOH solution, rebamipide loses the proton of the carboxylic acid group to form salt **1**. As shown in Figure 1, the asymmetric unit of salt **1** consists of one Na^+, one ethanol

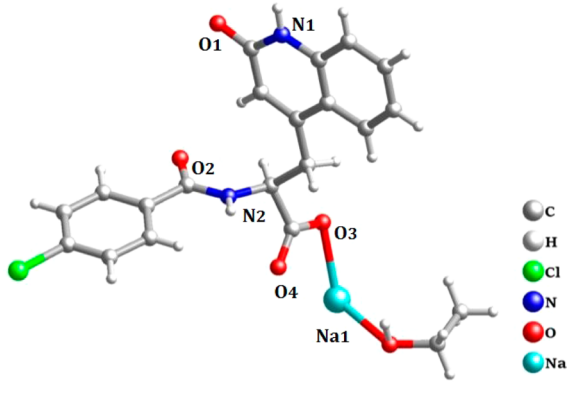

Figure 1. An asymmetric unit of salt **1**.

DOI: 10.1021/acs.cgd.5b01839
Cryst. Growth Des. XXXX, XXX, XXX−XXX

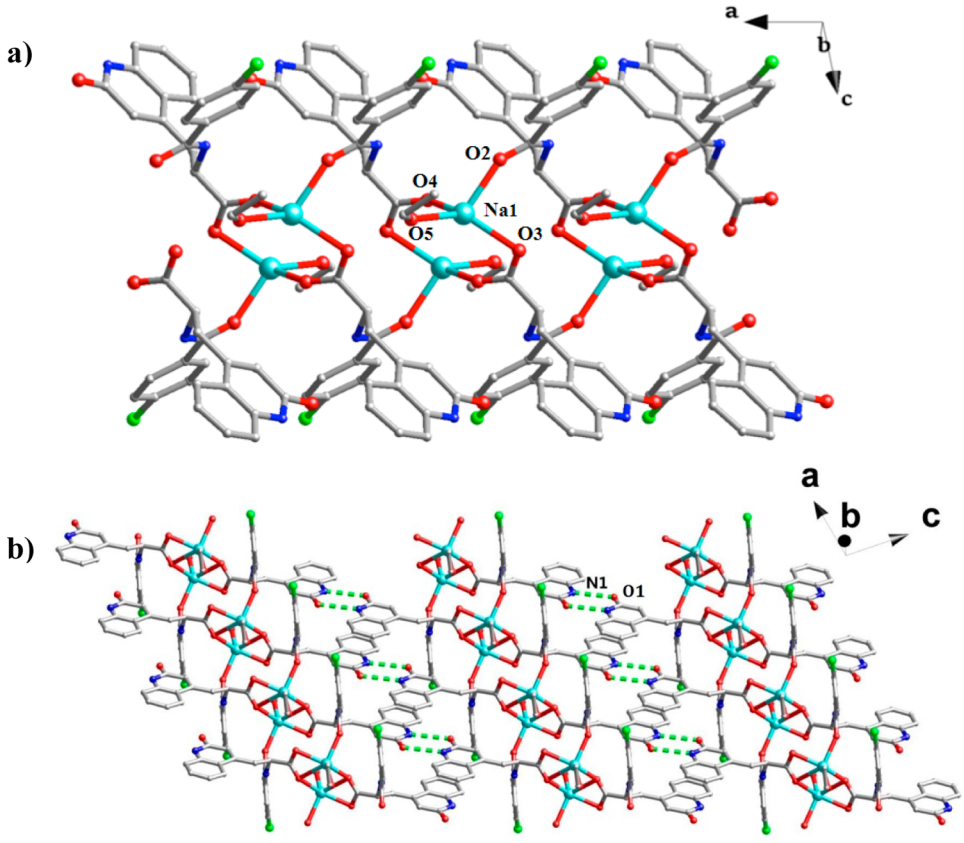

Figure 2. (a) 1D chain in salt **1**. (b) 2D supermolecular network formed by hydrogen bonding interactions of N1−H···O3. H atoms are omitted for the sake of clarity and green dashed lines represent the hydrogen bonding interactions.

molecule, and one $[HReb]^-$. In the rebamipide anion, the dihedral angle between quinolinone and chlorobenzene ring is 78.87°. The Na^+ ion exhibits a distorted tetrahedral geometry and coordinates with two oxygen atoms of carboxyl groups (O3, O4) from different drug molecules, one oxygen atom of acylamino group (O2), and one oxygen atom of ethanol (O5) (Figure 2a). Two Na^+ cations link two adjacent rebamipide ions to form an 8-membered ring. These 8-membered rings are connected by the Na1−O2 coordination bonds into a 1D chain along *a*-axis (Figure 2a). In this case, Na−O distances are in the range of 2.290−2.343 Å. In addition, N1−H···O1 hydrogen bond interactions extend the 1D chain into a 2D layer on the *ac*-plane (Figure 2b).

Crystal Structure of $Na_2(H_2O)_4(Reb)$ (2). When rebamipide reacts with NaOH aqueous under heating conditions, another sodium salt **2** is isolated. As shown in Figure 3, there are

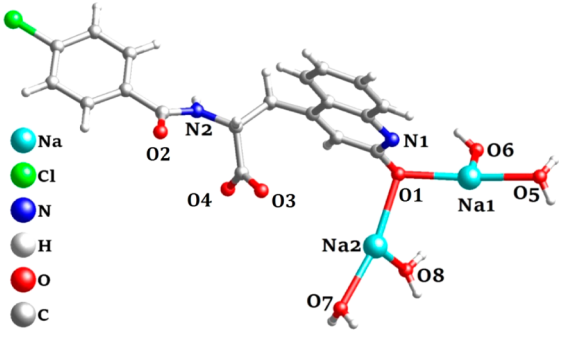

Figure 3. An asymmetric unit of salt **2**.

two Na^+, four coordinated water molecules, and one $[Reb]^{2-}$ in the asymmetric unit of **2**. Compared with **1**, two obvious differences are found in this case. First, prototropic tautomerism is observed in the quinolinone part and as a result the amide form transforms to an imidic acid form (Scheme 2). Second,

Scheme 2. Equilibrium between Two Tautomers

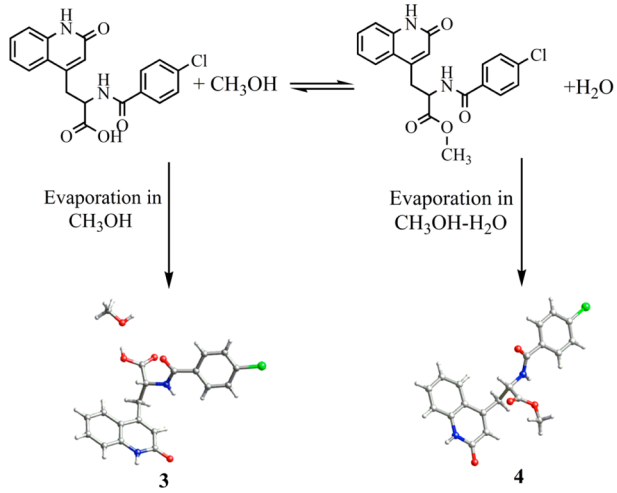

rebamipide loses two protons: one from a carboxyl group and the other from a hydroxyl group, to coordinate with sodium cations.

There are two crystallographically independent Na ions in **2**. Na1 coordinates with one carboxyl oxygen (O3), one hydroxyl oxygen (O1), and two water molecules (O5, O6) with

DOI: 10.1021/acs.cgd.5b01839
Cryst. Growth Des. XXXX, XXX, XXX−XXX

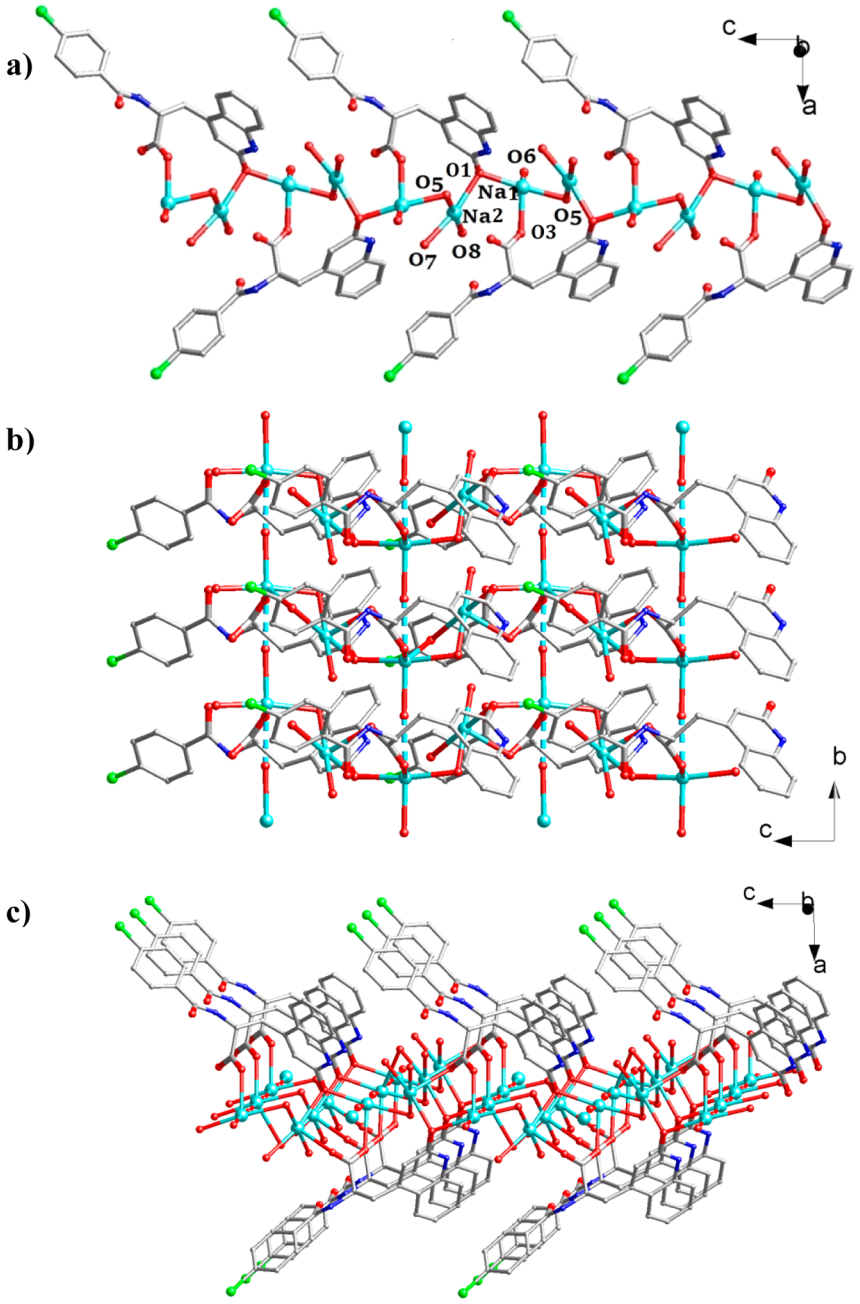

Figure 4. (a) 1D chain in salt **2**. (b) 2D sheet formed by Na···O weak interactions on *bc* plane. (c) The view of the 2D sheet along *b*-axis. H atoms are omitted for the sake of clarity and green-blue dashed lines represent the weak Na···O interactions.

seesaw-shaped geometry. Na2 adopts a distorted square geometry bonding with one hydroxyl oxygen (O1) and three water molecules (O5, O7, O8). The O1 and O5 acting as bridge link adjacent Na1 and Na2 ions into a 1D chain along *c*-axis (Figure 4a). The weak interaction of Na1···O6 with the distance of 2.710 Å further assembles 1D chains into a 2D sheet on the *ac*-plane (Figure 4b,c). Besides the Na···O weak interactions, a series of hydrogen bond interactions contribute to the formation of 2D sheet (Figure S2 and Table 2).

Crystal Structure of H_2Reb·CH_3OH (3). When rebamipide dissolve in methanol under solvothermal conditions, the crystals of solvate **3** were obtained. Asymmetric unit of **3** contains one rebamipide and one methanol molecule (Figure 5). The dihedral angle between quinolinone and chlorobenzene rings is 62.79°, which is less than the angles in salts **1** and **2**. As shown in Figure 6a, a 1D supermolecular chain is generated along *b*-axis with the help of N1−H···O3, O4−H···O5, and O5−H···O1 hydrogen bonds. The neighboring 1D chains are further connected via N2−H···O2 hydrogen bonds into a 2D sheet on the *bc*-plane (Figure 6).

Rebamipide Methyl Ester (4). When rebamipide dissolves in methanol-H_2O ($V_{methanl}$:V_{water} = 3:1), the crystals of rebamipide methyl ester **4** were obtained unexpectedly (Figure 7a). Rebamipide methyl ester as a prodrug has been synthesized through the reaction of rebamipide and methyl iodide.[33] However, in our case **4** is prepared by esterification of rebamipide with methanol. The dihedral angle between quinolinone and chlorobenzene rings in **4** (8.65°) is much smaller than those in **1**−**3**. As shown in Figure 7b, the N2−H···O2 hydrogen bonding interactions assemble the organic molecules into a 1D chain and

DOI: 10.1021/acs.cgd.5b01839
Cryst. Growth Des. XXXX, XXX, XXX−XXX

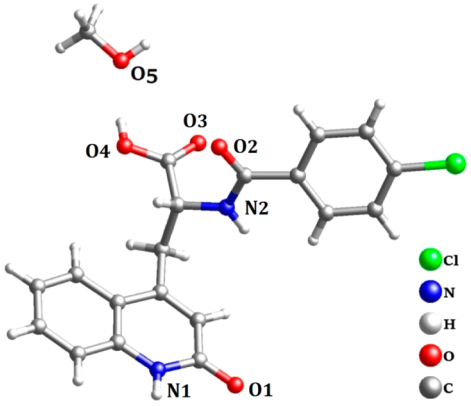

Figure 5. An asymmetric unit of solvate **3**.

two adjacent chains are further linked by N1−H···O1 hydrogen bondings to form a double supermolecular chain along *b*-axis.

The formation of rebamipide methyl ester is further proved by ^{1}H NMR (Figure S1). Through the comparison of rebamipide API and its methyl ester, it is clear that in **4** the active hydrogen of carboxyl group with δ = 13.0 disappears and an additional single peak of $-CH_3$ with δ = 3.69 is observed. Moreover, the rebamipide peaks are slightly shifted to higher field relative to the peaks of API, because of the electron-donating ability of the methyl group.

The Factors Influencing the Synthesis of 1−4. Although sodium salts **1** and **2** were all prepared by the reaction of rebamipide ethanol solution and NaOH aqueous, they have totally different structures. In order to explore the controlling factors, the adding order of starting material, the amount of NaOH, and reaction temperature were investigated (see Table S1). The results display that the formation of salt **1** or **2** depends on the temperature. As shown in Scheme 2, two tautomers, amide form (in **1**) and imidic acid form (in **2**), exist in a chemical equilibrium. Generally, the extra ratio of the isomers is influenced by temperature, solvent, and pH value.[34−37] The previous study shows that high temperature is beneficial for the formation of imidic acid form.[38] Therefore, the sodium salt **2** based on imidic acid form was isolated under heating conditions, while under room temperature the sodium salt **1** based on amide from was generated. Although the prototropic tautomerism is common in heterocycles, to the best of our knowledge, the imidic acid form of rebamipide has not been reported. Moreover, during our experiment even if the API solution was heated in temperature range of 120−160 °C, we still did not observe the formation of imidic acid form as neutral molecules. Therefore, we speculate that the salt forming process is helpful to stabilize the imidic acid form.

Compounds **3** and **4** are all crystallized from the rebamipide solution prepared under solvothermal conditions (120 °C for 48 h). The only difference is that the solvent used in **3** is methanol, but that in **4** is methanol-H_2O with volume ratio of 3:1. In **3**, methanol as a solvent is involved in the lattice, but in **4**, methanol acts as a reactant to form ester with API molecule. In order to explore the key factor controlling the formation of **3** and **4**, the reaction solutions of **3** and **4** are characterized by ESI-MS. The analyses of the positive mode mass spectra display that both API with m/z = 371.09 and methyl ester of rebamipide with m/z = 385. 09 are detected in solution and in the two cases the main products are all

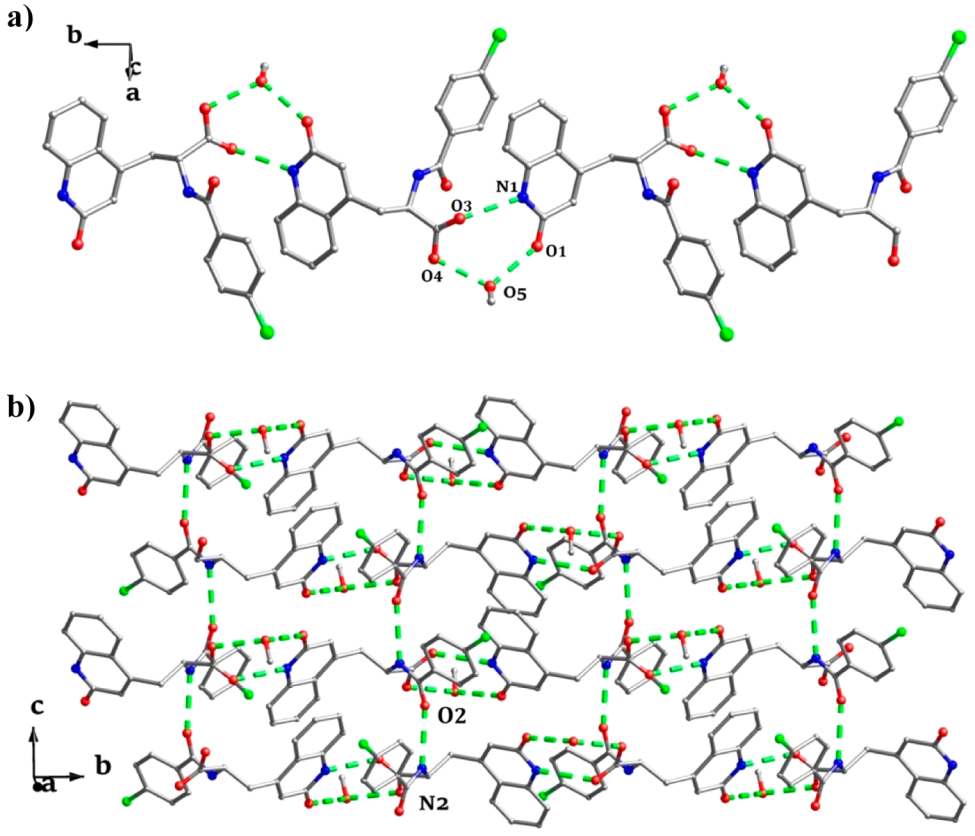

Figure 6. (a) 1D chain formed by hydrogen bonding in **3**. (b) 2D supermolecular network on *bc* plane. H atoms are omitted for the sake of clarity and green dashed lines represent the hydrogen bonding interactions.

DOI: 10.1021/acs.cgd.5b01839
Cryst. Growth Des. XXXX, XXX, XXX−XXX

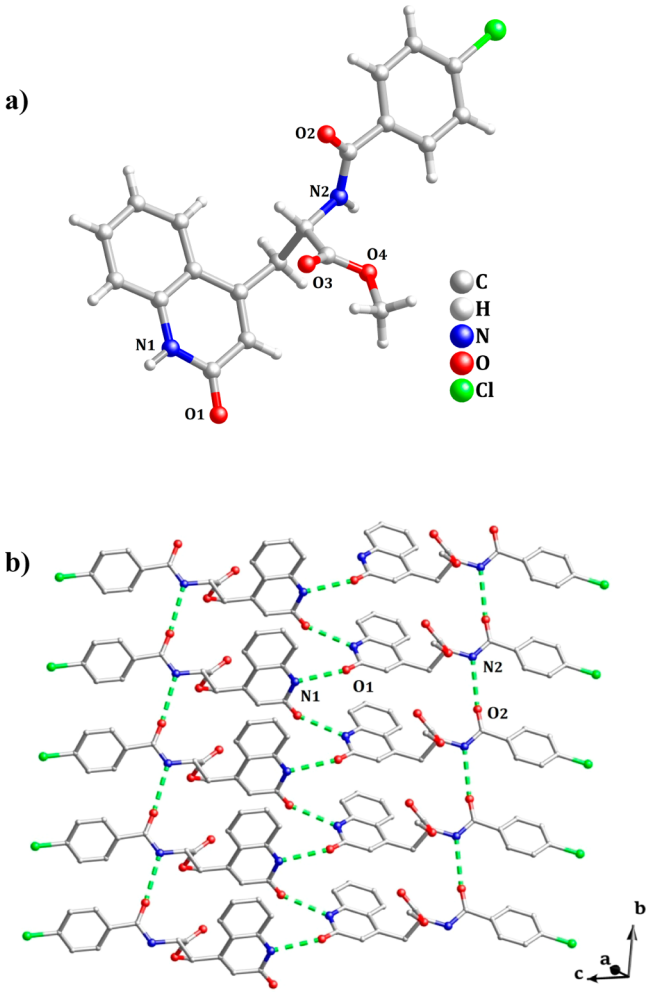

Figure 7. (a) An asymmetric unit of rebamipide methyl ester **4**. (b) 1D double chain assembled by hydrogen bonding interactions.

esters (Figure S3). Why we do not isolate ester during the synthesis of **3**? We speculate that solubility is the key factor controlling the crystallization of **3** and **4**. In methanol, the ester is more soluble than API, so during evaporation API combining with methanol first precipitates to form **3** (Scheme 3). As a result, the equilibrium goes backward and more solvate **3** is obtained. However, when deionic water was added, the solubility of ester dramatically decreases, so the ester precipitates instead (Scheme 3). With the precipitation of **4**, the equilibrium moves forward, followed by the crystallization of **4**. Therefore, the harvesting of **3** or **4** is controlled by the dynamics and the solubility of API or ester is adjusted by water.

Scheme 3. Equilibrium between Rebamipide and its Methyl Ester

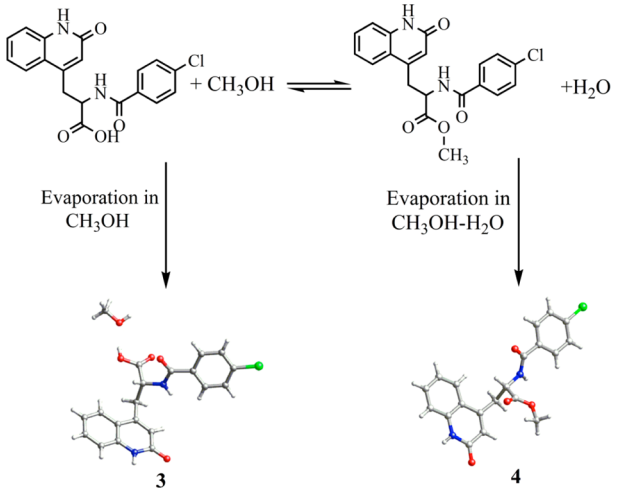

The Powder X-ray Diffraction and Thermal Analyses. PXRD is proved to be a reliable technique for assessment of solid forms in pharmaceutical study. As shown in Figure S4, the PXRD patterns of compounds **1**−**4** are obviously different from that of API, proving the formation of new solid forms. Moreover, the PXRD patterns of the synthesized samples closely match the simulated ones (Figure S5).

The thermal behaviors of API and compounds **1**−**4** were investigated by differential scanning calorimetry (DSC) and thermogravimetric analysis (TGA). The results are presented in Figure 8. In the DSC and TGA plots of **1**, an initial endotherm at 160 °C corresponds to a weight loss of ethanol molecule (obsd.10.40%, calc.10.49%), and the endotherm at 318 °C is attributed to the decomposition of **1**. For **2**, the TGA curve shows a weight loss of 14.70% in the 73−97 °C range, which is consistent with the loss of four water molecules (calc.14.79%). Then upon further heating, compound **2** decomposes at 267 °C. The first endothermic peak of **3** at 151 °C is for the loss of methanol molecular (obsd.7.98%, calc.7.95%) and **3** decomposes at 273 °C. The melting point of **4** is 269 °C and above this decomposition begins.

Spectral Analysis. The structure changes of drug molecules in **1**, **2**, and **4** are further confirmed by FT-IR spectroscopy. Generally, the characteristic absorption peak of −COOH group is at 1720−1700 cm^{-1}, whereas the ones of $-COO^-$ group are at 1650−1550 cm^{-1} (strong) and 1400 cm^{-1} (weak). The IR spectra of API and compounds **1**−**4** are shown in Figure S6. The strong absorption peak at 1720 cm^{-1} in API disappears in salts **1** and **2**. Instead, new absorption peaks arising from asymmetric and symmetric vibration of carboxylate group are observed at 1614 and 1395 cm^{-1} (for **1**) and 1612 and 1392 cm^{-1} (for **2**). Moreover, the characteristic absorption peaks of ester group at 1156 and 1088 cm^{-1} appear in the IR spectrum of **4**.

Dissolution Study and Stability. Powder dissolution profiles of rebamipide API and compounds **1**−**4** in simulated succus gastricus (HCl solution with pH = 1.2) are shown in Figure 9. It is found that both the dissolution rate and apparent solubilities of **1**−**4** are higher than those of API. All the compounds reach their maximum solubility (S_{max}) within 17 min and S_{max} is enhanced by 4.05, 4.73, 3.21, and 1.23 times for **1**−**4**, respectively, compared to that of API (Figure 9a). Then the solubilities of **1**−**3** began to decrease and after 36 h the solubility of each compound was close to that of API (Figure 9b). Similar phenomena have been reported by Lu T. B. et al.[17,22,39] The left solid samples of the dissolution experiments were collected and characterized by PXRD. The PXRD patterns display that compounds **1**−**3** transform to API under acid conditions (see Figure S7) and this transformation might lead to the decrease of solubility. The rapid dissolution behavior of **1**−**4** would be beneficial to their gastrointestinal absorption. The solid forms of **1** and **2** were found to be stable under ambient conditions (~25 °C and 30% relative humidity) for more than three months (see Supporting Information Figure S8). However, they are unstable under moisture conditions (40 °C and 75% relative humidity) as confirmed by PXRD results.

DOI: 10.1021/acs.cgd.5b01839
Cryst. Growth Des. XXXX, XXX, XXX−XXX

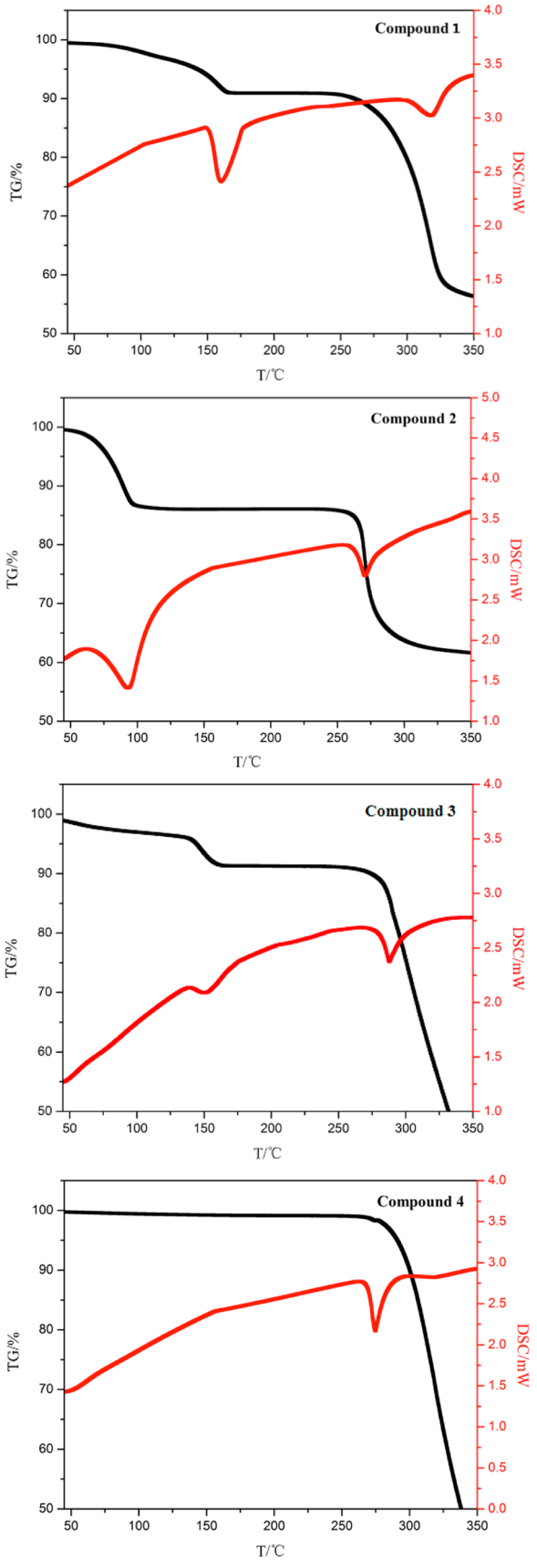

Figure 8. TG (black) and DSC (red) thermograms of compounds **1**−**4**.

Pharmacokinetic Study. The pharmacokinetic study (PK) of compounds **1**−**4** and original API was carried out in Wistar rats, which is a classic model to evaluate a drug's absorption. The mean plasma concentration vs time plots for rebamipide and compounds **1**−**4** after oral administration are shown in Figure 10. Three important PK parameters, maximal plasma concentration (C_{max}), the time required to reach the C_{max} (t_{max}), and the area under the curve (AUC), are present in Table 3.

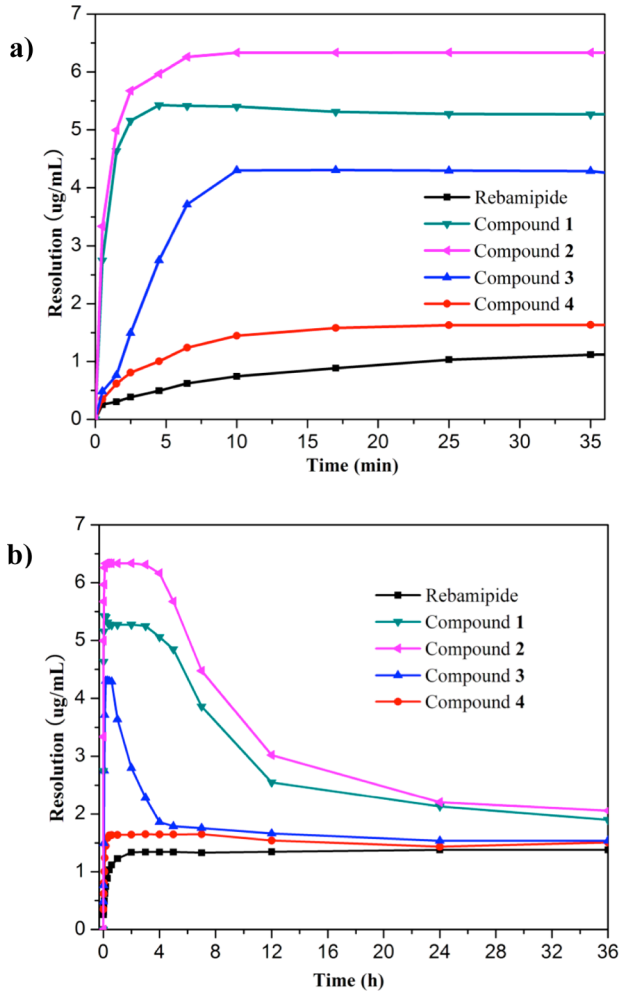

Figure 9. Dissolution profiles of API and compounds **1**−**4** in HCl solution (pH = 1.2) within (a) 35 min and (b) 36 h.

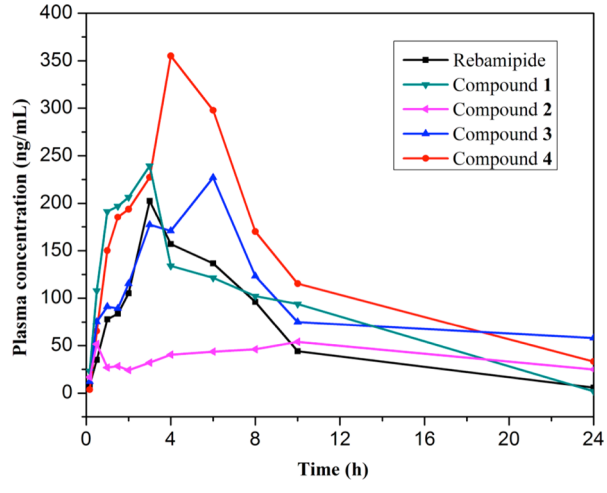

Figure 10. Mean plasma concentration vs time profiles of original API and compounds **1**−**4** in rats after oral administration.

DOI: 10.1021/acs.cgd.5b01839
Cryst. Growth Des. XXXX, XXX, XXX−XXX

Table 3. PK Data of the Original API and Compounds 1-4

drug	C_{max}(ng/mL)	t_{max}(h)	AUC (ng·h/mL)	F (%)
original API	202.5	3.00	1694.0	100.0
compound **1**	239.3	3.00	2052.4	121.2
compound **2**	53.82	0.50	948.20	56.00
compound **3**	227.2	6.00	2348.5	138.6
compound **4**	355.0	4.00	3229.8	190.7

In pharmacology, bioavailability is measured by the AUC value. Taking the $AUC_{0-\infty}$ of API as 100%, the relative bioavailability of **1**−**4** was calculated as 121.2, 56.00, 138.6, and 190.7%, respectively. The results indicate that the absorption of compounds **1**, **3**, or **4** upon oral administration is better than that of API. In addition, C_{max} value of **4** is increased by 1.8-fold. Rebamipide as a class IV drug faces two problems: low solubility and low permeability. For **4**, although its solubility is nearly the same as that of API, its absorption is superior to others as the permeability of the drug is enhanced by forming ester. Moreover, the in vivo experiments display that the methyl ester of rebamipide, **4**, rapidly and completely converts to the API because in the range of 0.17 to 24 h no methyl ester compound is detected. For **1** and **3**, the improvement of bioavailability is probably due to their good dissolution behavior. As for **2**, although its dissolution behavior is better than others, its absorption is poorer than others. We speculate that the poor absorption behavior of **2** might be relative to the formation of imidic acid tautomer (see Scheme 2) and its low permeability after forming salt.[40] The inconsistency of in vivo and in vitro experiments indicates that the in vivo environment is rather complex and the dissolution study is insufficient to accurately evaluate the absorption of a drug.

CONCLUSIONS

In this work, two sodium salts **1** and **2**, one solvate **3**, and methyl ester **4** of rebamipide have been synthesized and for the first time the crystal structures of this drug have been determined. The control experiments display that the controlling factor in the preparation of **1** and **2** is reaction temperature and the one in the synthesis of **3** and **4** is solubility of product. It is notable that the solubility and oral bioavailability of **1**, **3**, and **4** have been obviously improved, relative to those of API. Therefore, the three compounds could be potential candidates in the pharmaceutical industry. In addition, toxicity and efficacy studies continue in our laboratory.

ASSOCIATED CONTENT

Supporting Information

The Supporting Information is available free of charge on the ACS Publications website at DOI: 10.1021/acs.cgd.5b01839.

Additional measured and calculated PXRD patterns, IR spectra, ^{1}H NMR spectra, MS spectra, and the selected bond distances and angles (PDF)

Accession Codes

CCDC 1404894, 1404896, 1439500, and 1439505 contain the supplementary crystallographic data for this paper. These data can be obtained free of charge via www.ccdc.cam.ac.uk/data_request/cif, or by emailing data_request@ccdc.cam.ac.uk, or by contacting The Cambridge Crystallographic Data Centre, 12, Union Road, Cambridge CB2 1EZ, UK; fax: +44 1223 336033.

AUTHOR INFORMATION

Corresponding Authors

*E-mail: gujk@jlu.edu.cn.
*E-mail: cwhu@bit.edu.cn.

Author Contributions

‖Y.C. and C.L. contributed equally to this work.

Notes

The authors declare no competing financial interest.

ACKNOWLEDGMENTS

This work was financially supported by the NSFC (21231002, 21276026, 21173021, 21371024, 81430087), the 111 Project (B07012), and 973 Program (2014CB932103).

REFERENCES

(1) Uchida, M.; Tabusa, F.; Komatsu, M.; Morita, S.; Kanbe, T.; Nakagawa, K. *Chem. Pharm. Bull.* **1985**, *33*, 3775−3786.
(2) Arakawa, T.; Kobayashi, K.; Yoshikawa, T.; Tarnawski, A. *Dig. Dis. Sci.* **1998**, *43*, 5S−13S.
(3) Kashima, T.; Itakura, H.; Akiyama, H.; Kishi, S. *Clin. Ophthalmol.* **2014**, *8*, 1003−1010.
(4) Watanabe, T.; Takeuchi, T.; Handa, O.; Sakata, Y.; Tanigawa, T.; Shiba, M.; Naito, Y.; Higuchi, K.; Fujimoto, K.; Yoshikawa, T.; Arakawa, T. *PLoS One* **2015**, *10*, e0122330−e0122312.
(5) Shinohara, A.; Nakamura, M.; Onikubo, T.; Nakamura, K. *Yakugaku Zasshi* **2015**, *135*, 937−941.
(6) Miyake, M.; Oka, Y.; Minami, T.; Toguchi, H.; Odomi, M.; Ogawara, K.-I.; Higaki, K.; Kimura, T. *J. Pharm. Sci.* **2003**, *92*, 911−921.
(7) Pradhan, R.; Tran, T. H.; Choi, J. Y.; Choi, I. S.; Choi, H.-G.; Yong, C. S.; Kim, J. O. *Arch. Pharmacal Res.* **2015**, *38*, 522−533.
(8) Shioya, Y.; Kashiyama, E.; Okada, K.; Kusumoto, N.; Abe, Y.; Uchida, M.; Shimizu, T. *Iyakuhin Kenkyu* **1989**, *20*, 522−533.
(9) Singhal, D.; Curatolo, W. *Adv. Drug Delivery Rev.* **2004**, *56*, 335−347.
(10) Schultheiss, N.; Newman, A. *Cryst. Growth Des.* **2009**, *9*, 2950−2967.
(11) Rodriguez-Spong, B.; Price, C. P.; Jayasankar, A.; Matzger, A. J.; Rodriguez-Hornedo, N. *Adv. Drug Delivery Rev.* **2004**, *56*, 241−274.
(12) Gangavaram, S.; Raghavender, S.; Sanphui, P.; Pal, S.; Manjunatha, S. G.; Nambiar, S.; Nangia, A. *Cryst. Growth Des.* **2012**, *12*, 4963−4971.
(13) Maddileti, D.; Swapna, B.; Nangia, A. *Cryst. Growth Des.* **2015**, *15*, 1745−1756.
(14) Braun, D. E.; Gelbrich, T.; Kahlenberg, V.; Tessadri, R.; Wieser, J.; Griesser, U. J. *Cryst. Growth Des.* **2009**, *9*, 1054−1065.
(15) Sanphui, P.; Devi, V. K.; Clara, D.; Malviya, N.; Ganguly, S.; Desiraju, G. R. *Mol. Pharmaceutics* **2015**, *12*, 1615−1622.
(16) Tao, Q.; Chen, J.-M.; Ma, L.; Lu, T.-B. *Cryst. Growth Des.* **2012**, *12*, 3144−3152.
(17) Yan, Y.; Chen, J.-M.; Geng, N.; Lu, T.-B. *Cryst. Growth Des.* **2012**, *12*, 2226−2233.
(18) Zheng, S.-L.; Chen, J.-M.; Zhang, W.-X.; Lu, T.-B. *Cryst. Growth Des.* **2011**, *11*, 466−471.
(19) Prado, L. D.; Rocha, H. V. A.; Resende, J. A. L. C.; Ferreira, G. B.; Teixeira, A. M. R. d. F. *CrystEngComm* **2014**, *16*, 3168−3179.
(20) Karanam, M.; Choudhury, A. R. *Cryst. Growth Des.* **2013**, *13*, 1626−1637.
(21) Song, J.-X.; Yan, Y.; Yao, J.; Chen, J.-M.; Lu, T.-B. *Cryst. Growth Des.* **2014**, *14*, 3069−3077.
(22) Xu, L.-L.; Chen, J.-M.; Yan, Y.; Lu, T.-B. *Cryst. Growth Des.* **2012**, *12*, 6004−6011.
(23) Zhang, T.; Yang, Y.; Wang, H.; Sun, F.; Zhao, X.; Jia, J.; Liu, J.; Guo, W.; Cui, X.; Gu, J.; Zhu, G. *Cryst. Growth Des.* **2013**, *13*, 5261−5266.
(24) Zhang, T.; Yang, Y.; Zhao, X.; Jia, J.; Su, H.; He, H.; Gu, J.; Zhu, G. *CrystEngComm* **2014**, *16*, 7667−7672.

DOI: 10.1021/acs.cgd.5b01839
Cryst. Growth Des. XXXX, XXX, XXX−XXX

(25) Chi, Y.; Xu, W.; Yang, Y.; Yang, Z.; Lv, H.; Yang, S.; Lin, Z.; Li, J.; Gu, J.; Hill, C. L.; Hu, C. *Cryst. Growth Des.* **2015**, *15*, 3707−3714.
(26) Zeng, X.; Jia, C. Rebamipide monohydrate crystal form and preparation method thereof. China Patent CN 104418802, March 18, 2015.
(27) Holland, J.; Gooding, D.; Chorlton, A. Novel rebamipide complexes and cocrystals. Patent, PCT Int. Appl. WO 2012114317, August 30, 2012.
(28) Beijing Fukangren Bio-Pharm Technology Co., Ltd. Officinal composite using Rebamipide officinal salt as active ingredient. China Patent CN 102512420, June 27, 2011.
(29) Aitipamula, S.; Wong, A. B. H.; Chow, P. S.; Tan, R. B. H. *Cryst. Growth Des.* **2014**, *14*, 2542−2556.
(30) Chen, J.-M.; Wang, Z.-Z.; Wu, C.-B.; Li, S.; Lu, T.-B. *CrystEngComm* **2012**, *14*, 6221−6229.
(31) Rao Khandavilli, U. B.; Gangavaram, S.; Rajesh Goud, N.; Cherukuvada, S.; Raghavender, S.; Nangia, A.; Manjunatha, S. G.; Nambiar, S.; Pal, S. *CrystEngComm* **2014**, *16*, 4842−4852.
(32) M, S. G. *SHELXL97, Program for the Refinement of Crystal Structure*; University of Göttingen: Göttingen, Germany, 1997.
(33) Hayashi, S.; Sugiyama, T.; Amano, K.-I.; Isogai, H.; Isogai, E.; Aihara, M.; Kikuchi, M.; Asaka, M.; Yokota, K.; Oguma, K.; Fujii, N.; Hirai, Y. *Antimicrob. Agents Chemother.* **1998**, *42*, 1895−1899.
(34) Balabin, R. M. *J. Chem. Phys.* **2009**, *131*, 154307−154308.
(35) El-Gendy, B. E.-D. M.; Katritzky, A. R.; Hall, C. D.; Draghici, B. *Abstracts of Papers*, 240th National Meeting of the American Chemical Society, Boston, MA, Aug 22−26, 2010; American Chemical Society: Washington, DC, 2010; COMP 15.
(36) Ivanova, D.; Deneva, V.; Nedeltcheva, D.; Kamounah, F. S.; Gergov, G.; Hansen, P. E.; Kawauchi, S.; Antonov, L. *RSC Adv.* **2015**, *5*, 31852−31860.
(37) Valadbeigi, Y.; Ilbeigi, V.; Tabrizchi, M. *Comput. Theor. Chem.* **2015**, *1061*, 27−35.
(38) Beak, P. *Acc. Chem. Res.* **1977**, *10*, 186−192.
(39) Geng, N.; Chen, J.-M.; Li, Z.-J.; Jiang, L.; Lu, T.-B. *Cryst. Growth Des.* **2013**, *13*, 3546−3553.
(40) Porter, W. R. *J. Comput.-Aided Mol. Des.* **2010**, *24*, 553−573.

DOI: 10.1021/acs.cgd.5b01839
Cryst. Growth Des. XXXX, XXX, XXX−XXX